How Different DNA-Binding Proteins Affect Long-Range Oxidative Damage to DNA†

Scott R. Rajski‡ and Jacqueline K. Barton*

Division of Chemistry and Chemical Engineering, California Institute of Technology, Pasadena, California 91125

Received November 22, 2000; Revised Manuscript Received March 1, 2001

ABSTRACT: Here the effect on DNA-mediated charge transport of binding by a variety of proteins is examined. DNA assemblies were constructed that contain a tethered rhodium intercalator, as photooxidant, as well as two 5′-GG-3′ sites flanking the DNA-binding site for the different proteins. By monitoring the ratio of oxidative damage promoted at the guanine doublet situated distal to the protein-binding site versus that at the proximal site as a function of protein binding, the effects of binding the proteins on DNA-mediated charge transport were determined. Proteins examined included both the wild-type and mutant methyltransferase, M.*Hha*I, which are base-flipping enzymes, the restriction endonuclease R.*Pvu*II, a TATA-binding protein, which kinks the DNA, and the transcription factor Antennapedia homeodomain protein, which binds DNA through a helix−turn−helix motif. In general, it was observed that yields of long-range oxidative damage correlate with protein-dependent alterations in DNA base stacking. Interactions that disturb the DNA π-stack inhibit DNA charge transport. Alternatively, interactions that promote no helix distortion but, as a result of tight packing, may rigidify the π-stack, serve instead to enhance the ability of the DNA base pairs to serve as a conduit for charge transport. Thus, protein binding to DNA modulates long-range charge transport both negatively and positively, depending upon the specific protein/DNA interactions in play. Long-range DNA charge transport and this modulation by protein binding may be important to consider physiologically.

DNA charge transport (CT)[1] chemistry has been the subject of considerable interest, particularly with respect to possible biological consequences (*1*). Charge migration through the DNA base stack has been shown to result in oxidative damage to guanine sites ~200 Å from the site of a remotely bound oxidant (*2*). Moreover, this oxidative damage from a distance depends on the intervening sequence of DNA bases and their dynamic structure (*3*). We have found in general that DNA-mediated charge transport and the oxidative damage that results are exquisitely sensitive to variations in the sequence- and conformation-dependent stacking of the intervening bases.

Oxidative damage to DNA from a distance has been probed in experiments from several laboratories using DNA assemblies constructed to contain a site-specifically-bound oxidant positioned at a site distant from that being oxidized (*1*). Both experimental methods and ab initio calculations reveal that 5′-G residues of 5′-GG-3′ steps are the most easily oxidized sites within DNA (*4*). This has been interpreted in terms of the localization of the 5′-GG-3′ dinucleotide HOMO at the 5′-G. It has also been proposed that the radical cation hole at the 5′-position within the DNA duplex may be stabilized as a result of overlap with the N7 nitrogen and O6 oxygen of the 3′-G (*5*). Once localized to the 5′-G, irreversible trapping of the radical by reaction with water and oxygen can occur on the millisecond time scale, so as to yield a mixture of oxidative lesions. The yield of these oxidative lesions is then commonly assayed as strand breaks in biochemical experiments using gel electrophoresis.

The first experiments demonstrating oxidative damage to DNA from a distance were carried out with a rhodium intercalator, $[Rh(phi)_2(bpy')]^{3+}$, where phi = 9,10-phenanthrenequinone diimine and bpy′ = 4-butyric acid, 4′-methylbipyridine, as the tethered photooxidant (*6*). Since then, using a combination of phosphoramidite chemistries and amide coupling-based strategies, a variety of DNA-bound photooxidants have been employed. We have, for example, also exploited a ruthenium intercalator, $Ru(phen)(bpy')(dppz)^{3+}$, where dppz = dipyridophenazine, generated in situ through a flash−quench strategy (*7*). Additionally, long-range oxidative damage at the 5′-G of 5′-GG-3′ sequences has been accomplished through generation of intercalated or end-capped anthraquinone radicals (*8*), sugar C4 radicals (by homolysis of C4 pivaloyl nucleotides) (*9*), photoactivated cyano-benzophenone-based uridine moieties (*10*), intercalated ethidium radical species (*11*), and naphthalimides (*12*).

Using both photophysical and biochemical methods, we have found DNA-mediated charge transport to be exquisitely sensitive to π-stacking, both of the donor/acceptor pair and

† Supported by NIH Grant GM49216.

* To whom correspondence should be addressed.

‡ Supported by a postdoctoral fellowship from the American Cancer Society.

[1] Abbreviations: CT, charge transport; bpy′, 4-butyric acid, 4′-methylbipyridine; phi, 9,10-phenanthrenequinone diimine; dppz, dipyridophenazine; phen, 1,10-phenanthrene; DPAGE, denaturing polyacrylamide gel electrophoresis; EDTA, ethylenediaminetetraacetic acid; SAH, *S*-adenosyl-L-homocysteine; Kphos, $KHPO_4$; DC, dark control; GLN237, wild-type M.*Hha*I; TRP237, M.*Hha*I Q237W; 4-MeI, 4-methylindole deoxyribonucleotide; TBP, TATA box binding protein; ANTP, Antennapedia homeodomain protein

10.1021/bi002684t CCC: $20.00
Published on Web 04/12/2001

of the intervening bases. Indeed, while measurements of long-range oxidative damage to DNA have been useful in probing DNA mechanistically, such studies can provide sensitive probes of DNA conformation and stacking (*3*). For example, the presence of a bulge in DNA, which is known to kink the DNA base stack, can attenuate long-range oxidative damage.

In this context, we probed earlier how the binding of a site-specifically-bound base-flipping enzyme, the methylase M.*Hha*I, might affect DNA-mediated charge transport (*13*). In these studies, hole transport was initiated by activation of intercalated $[Rh(phi)_2(bpy')]^{3+}$ tethered near the duplex terminus, and long-range oxidative damage from the rhodium photooxidant was measured at two 5′-GG-3′ sites incorporated on either side of the protein-binding consensus sequence. Thus, in these assemblies, measurements of the ratio of damage at the 5′-GG-3′ distal to the metal intercalation site from the site of protein binding compared with damage found at the proximal 5′-GG-3′ site provided a facile means by which to examine the influence on charge tranport of protein binding to an intervening binding site.

Our experiments with M.*Hha*I have been important not only in demonstrating how DNA-binding proteins may inhibit charge transport by introducing local interruptions in the π-stack, but also in illustrating how their binding may facilitate charge transport. Characterized crystallographically, the enzyme binds the sequence 5′-G<u>C</u>GC-3′ and effects methylation at each of the internal cytosines (underlined) (*14*). To gain access to each target cytosine for methylation, the enzyme extrudes the cytosine from the DNA helix. A key feature of the base-flipped complex is the insertion of GLN237 within the DNA cavity created with extrusion of the cytosine (*15*). The discontinuity of the DNA base stack at the site of base flipping with GLN237 insertion then serves to inhibit long-range charge transport (*13*). However, we also examined the effects of binding a TRP237 mutant, M.*Hha*I Q237W. Consistent with the notion that charge transport proceeds through the π-stack, inserting the aromatic indole side chain of a tryptophan (Trp) residue into the DNA pocket actually restores long-range damage. We furthermore applied transient absorption spectroscopy to probe charge transport in ruthenium-modified assemblies containing the bound M.*Hha*I Q237W (*16*). These spectroscopic assays established directly the formation of transient radical species having both tryptophan and guanine radical character. In general, then, these studies exemplified how DNA-binding proteins might play a role both as inhibitor and as activator of DNA-mediated charge transport, and, indeed, how DNA-binding proteins might participate in DNA charge transport chemistry.

Here we extend our studies of how proteins may affect long-range charge transport through DNA so as to include a variety of proteins which bind DNA in different modes. We have focused our studies, in general, on structurally well-characterized nucleoprotein interactions so as to relate the protein-dependent changes in π-stacking to measurements of long-range oxidative damage. Biochemical methods are used to probe the influence of protein binding on long-range oxidative damage. The results described here underscore the key requirement of π-stacking along the path for DNA charge transport and how proteins that affect the π-stacked structure of DNA, both statically and dynamically, can influence electronic coupling within the DNA helix.

EXPERIMENTAL PROCEDURES

Materials

All oligonucleotides were prepared on an Applied Biosystems 394 DNA synthesizer using DMT off and the manual cleavage mode (*17*). Unmetalated DNA was then deprotected by heating to 60 °C in concentrated NH_4OH for 10 h. Following deprotection, samples were dried in vacuo, and then purified by 10% denaturing gel electrophoresis (DPAGE). Following DPAGE, DNA bands were visualized by UV shadowing, excised, and isolated by crushing and soaking into 500 mM NH_4OAc/1 mM EDTA (pH 8.0) for 6 h at ambient temperature. Samples were filtered through Centrex 0.45 μm nitrocellulose and filtrates then isolated by C18 Sep-Pak. Samples were dried in vacuo and then resuspended into DDH_2O, and the pH was set to 8 with 0.01 M NaOH. The concentration of single-stranded oligonucleotides in aqueous solution was determined by UV−visible spectroscopy on a Beckman DU 7400 Spectrophotometer; ϵ (260 nm, M^{-1} cm^{-1}) adenine = 15 400; guanine = 11 500, cytosine = 7400, thymine = 8700. $[Rh(phi)_2(bpy')]^{3+}$ was prepared according to previously published procedures as was the preparation of oligonucleotides with appended rhodium intercalalators (*18*). Rh−DNA conjugates were purified by successive rounds of HPLC. Subsequent HPLC analysis revealed these conditions to yield material of ≥98% purity. This was verified by UV−Vis and Maldi-TOF mass spectrometry.

Unmetalated oligonucleotides were labeled by addition of a 5′-^{32}P-labeled phosphate using polynucleotide kinase. Following incubation at 37 °C, polynucleotide kinase was deactivated by heating to 70 °C for 10 min. Samples were then dried in vacuo, and resuspended into DPAGE loading dye. Samples were heated to 90 °C for 5 min and loaded to a pre-run 10% denaturing polyacrylamide gel, and electrophoresis was conducted at 75 W for ∼3 h. DNA bands were visualized by autoradiography, excised from the gel, and soaked in buffer for 8−12 h. Supernatants were triturated away from gel slices; then butanol extracted down to a volume of 100 μL. Samples were then desalted by passage through Sephadex G-50 size exclusion resin and then dried in vacuo. These radiolabeled strands were used in combination with unlabeled strand and their metalated complements to generate stock solutions typically ∼2 μM duplex in 25 mM NH_4OAc, pH ∼8.5. All solutions were typically stored at −80 °C until further use.

Methods

All irradiations were performed at ambient temperature on 10 μL samples in pre-siliconized 1.5 mL Eppendorf tubes using a 1000 W Hg/Xe arc lamp with a monochromator. Irradiations were conducted at 365 nm for 1 h. For each irradiation performed, a parallel reaction containing the identical buffer and/or enzyme composition was conducted in which the sample was kept shielded from light for a period of 1 h. These "dark control" (DC) reactions were piperidine-digested and analyzed in a fashion identical to that used for irradiated samples. Following irradiation, samples were ethanol-precipitated and then piperidine-digested or simply piperidine-digested directly. Specific reaction/binding conditions and workup procedures for the different systems are given below.

M.HhaI Complex Binding/Irradiations. All reactions were 200 nM in duplex Rh−DNA assembly. Enzyme concentrations were ramped from 0 to 3200 nM with all binding/irradiations conducted in the presence of 25 mM NH_4OAc (pH 9.0), 1 mM Kphos (pH 7.4), 5 mM NaCl, 50 μM EDTA, 5% glycerol, 200 nM SAH, and a 40-fold molar excess (in base pairs) of poly(dA)-poly(dT). Following irradiations, samples were brought to a volume of 100 μL in 1 M piperidine, and samples were then heated at 85 °C for 30 min followed by freezing and overnight lyophilization. Samples were resuspended into denaturing gel electrophoresis loading dye to a specific activity of 5000−10 000 cpm/μL, and 20% denaturing gel electrophoresis was carried out on 40 000 cpm per reaction. Images of the gels were obtained by phosphorimagery (Molecular Dynamics) and analyzed using ImageQuant software. For gel shift analysis, binding reactions were conducted for 30 min at ambient temperature followed by loading of 5 μL aliquots to a running 10% native polyacrylamide gel. Electrophoresis at 250 V for 2.5 h was conducted at 4 °C.

TATA Box Binding Protein−DNA Complex Binding/Irradiations. All reactions were 100 nM in duplex Rh−DNA assembly. Enzyme concentrations were ramped from 0 to 910 nM with all binding/irradiations conducted in the presence of 20 mM Tris (pH 7.5), 4 mM spermidine, 75 mM potassium glutamate, 0.1 mM EDTA, 4 mM $MgCl_2$, 13.6 μM poly(dG-dC) (in nucleotides), 0.01% NP-40, 5 μg/mL BSA, 5% glycerol. All reactions (DC and irradiation samples) were incubated at ambient temperature for 1 h prior to irradiation or further "dark" digestion. Following irradiations (or dark digestion), samples were brought to a volume of 100 μL in H_2O, and DNA strands were ethanol-precipitated. Liquid scintillation counting revealed less than a 2% loss of radiolabeled material. Following precipitation, DNA pellets were dissolved into 100 μL of 1 M piperidine and heated at 90 °C for 30 min. Samples were resuspended into denaturing gel electrophoresis loading dye to a specific activity of 10 000 cpm/μL, and 20% denaturing gel electrophoresis was carried out on 40 000 cpm per reaction.

4-MeI Experiments. Irradiations were conducted on solutions 200 nM in duplex DNA under buffer conditions identical to those used for M.*Hha*I experiments (vide supra). Following irradiation, samples were brought to a volume of 100 μL with 1 M piperidine. Samples were then heated at 85 °C for 30 min followed by freezing and overnight lyophilization. Analysis of damage was analogous to the methods described for M.*Hha*I-binding reactions.

M.PvuII Complex Binding/Irradiations. All reactions were 180 nM in duplex Rh−DNA assembly. Enzyme concentrations were ramped from 0 to 3.91 μM R.*Pvu*II, respectively. Both oxidative damage and gel shift trials were 180 nM in Rh−DNA assembly and contained 4.5 mM NH_4OAc (pH 8.5), 23 nM poly(dI)-poly(dC) (in base pairs), 9 mM $CaCl_2$, 1.36 mM Kphos, 6.7 mM NaCl, 50 μM EDTA, 6% glycerol. Following incubation (±light), samples were brought to 100 μL volume with H_2O followed by ethanol precipitation and digestion at 90 °C with 100 μL of 1 M piperidine for 30 min. Data were analyzed as for the M.*Hha*I experiments.

ANTP Complex Binding/Irradiations. [Rh−DNA] ranged from 181 to 154 nM in duplex with a variation in enzyme concentration of 980 nM−2.9 μM. Buffer conditions were 2.1 mM NH_4OAc (pH 8.5), 1.7 mM Kphos, 8.3 mM NaCl, 80 μM EDTA, 8% glycerol. Following incubation (±light), samples were brought to 100 μL volume with H_2O followed by ethanol precipitation and digestion at 90 °C with 1 M piperidine for 30 min.

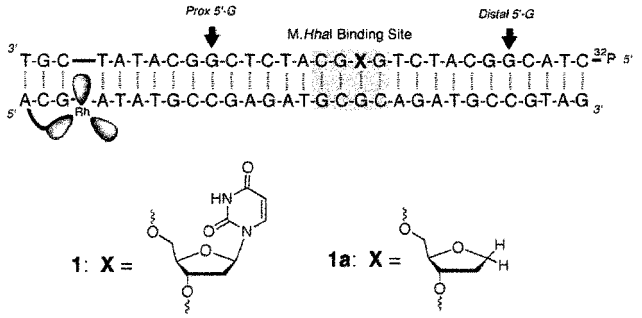

FIGURE 1: Rh−DNA assemblies bearing the M.*Hha*I recognition sequence 5′-GXGC-3′ where X = uracil or an abasic site on the ^{32}P-labeled strand and 5′-GCGC-3′ is on the Rh-tethered strand. The rhodium intercalator tethered to the DNA is $[Rh(phi)_2(bpy')]^{3+}$, and photocleavage studies indicate the primary site of intercalation to be that shown.

Gel Mobility Shift Assays. Radiolabeled DNA stock solutions were prepared as previously described for long-range charge-transfer experiments. Buffering conditions for each unique protein−DNA system were as noted for the irradiation procedures (vide supra). All EMSA experiments were performed at 4 °C with samples being loaded only after a pre-run time of ~1 h at the same current used for the experiment. Binding reactions were conducted at ambient temperature for a period of 30 min, after which time 5 μL reaction aliquots were withdrawn and loaded directly to the gel. Critically, samples were loaded with concomitant application of current so as to ensure equal and minimum residency times of each sample within the well prior to migration into the gel matrix. Just as native gel electrophoresis (250 V for 2 h in 0.5× TBE) was conducted at 4 °C, so too was sample application. Notably, R.*Pvu*II gel shift analyses required the presence of 5 mM $CaCl_2$ in the 0.5× TBE electrophoresis buffer. These conditions afforded a high degree of resolution between unbound duplex and protein-bound duplex oligodeoxyribonucleotides. Gels were dried under vacuum (80 °C for 2 h) and then exposed to phosphorimage plates for a period of 12 h at ambient temperature. Images were recorded using ImageQuant software in combination with Molecular Dynamics Phosphorimaging hardware.

RESULTS

Effects on DNA Charge Transport of Binding Wild-Type and Mutant M.HhaI. Figure 1 shows two $[Rh(phi)_2(dmb)]^{3+}$-tethered DNA assemblies used to explore how M.*Hha*I modulates oxidative damage to DNA from a distance. As for all such assays, the assemblies contain, in addition to the tethered rhodium intercalator, two 5′-GG-3′ sites flanking the protein-binding site. For assembly **1**, the protein-binding site contains a G-U mismatch at the site of base flipping; the incorporation of such mismatches inhibits protein dissociation (*19*). Alternatively, assembly **1a** contains an abasic site; the tetrahydrofuran structure promotes enzyme-facilitated flipping of the abasic sugar moiety (*20*). Figure 2 shows representative data for the effects of binding both wild-type and M.*Hha*I Q237W to **1** on long-range charge transport.

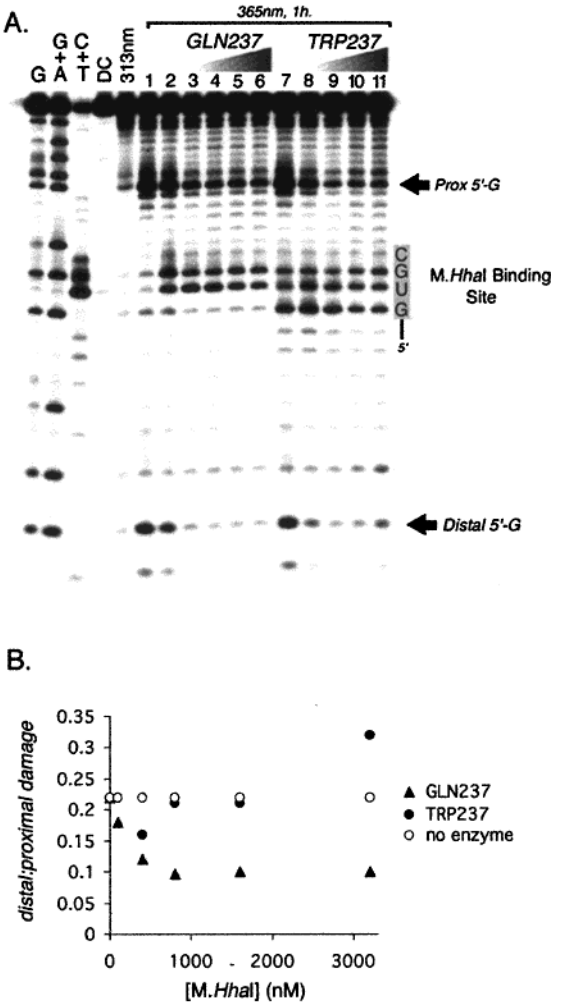

FIGURE 2: Photooxidative damage as a function of wild-type and mutant M.*Hha*I concentration. In (A), the 5′-^{32}P-end-labeled DNAs as visualized by phosphorimagery following irradiation, piperidine digestion, and 20% denaturing polyacrylamide gel electrophoresis are shown. Lanes with Maxam−Gilbert sequencing reactions, assembly **1** without irradiation (DC), and the duplex irradiated at both 313 nm and 365 nm but without M.*Hha*I are as noted. Lanes 2−6 and 7−11 contained 100, 400, 800, 1600, and 3200 nM native M.*Hha*I and tryptophan mutant M.*Hha*I, respectively. All samples contained 25 mM NH_4OAc (pH 9.0), 1 mM Kphos (pH 7.4), 5 mM NaCl, 50 μM EDTA, 5% glycerol, 200 nM SAH, 200 nM **1**, and a 40-fold molar excess (in base pairs) of poly(dA)-poly(dT). Irradiations were performed for 1 h at 365 nm using a 1000 W Hg/Xe lamp with a monochromator at 25 °C. The sites of rhodium intercalation appear as the band doubling near the native DNA band. Sites of proximal and distal 5′-GG-3′ damage are shown. In (B), the ratio of distal/proximal guanine damage is plotted as a function of added protein concentration.

As can be both seen in the gel and quantitated in the companion plot of distal/proximal guanine damage versus protein concentration, binding of the wild-type enzyme to the intervening site serves to inhibit long-range charge transport. In the presence of wild-type enzyme, one observes a significant diminution in oxidative damage at the distal 5′-GG-3′ doublet. Binding of M.*Hha*I Q237W to **1**, in contrast, restores long-range CT, as is also evident in the gel and companion plot. Indeed, under conditions of high M.*Hha*I Q237W concentration, an increase in the efficiency of CT over reactions without enzyme was observed. This increase may reflect a decrease in base motions associated with the transient packing of multiple M.*Hha*I Q237W proteins nonspecifically.

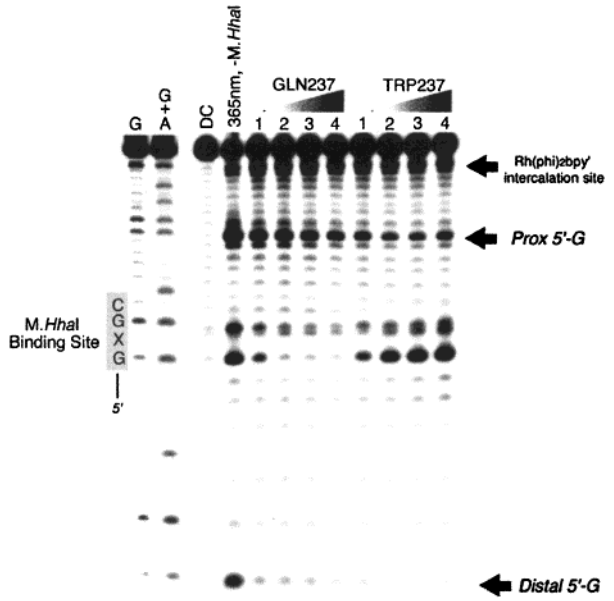

FIGURE 3: Long-range charge-transfer reactions of **1a** in the presence of either wild-type M.*Hha*I or M.*Hha*I Q237W. The concentrations of DNA and buffer are identical to those for Figure 2. Maxam−Gilbert reactions, dark control (DC), and 365 nm light standards are as noted above the appropriate lanes. Concentrations of enzyme were varied from 100, to 400, to 800, to 1600 nM in lanes 1−4. Irradiations were performed for 1 h at 365 nm at 25 °C.

As shown in Figure 3, we also examined the effects of M.*Hha*I binding to assembly **1a**, containing an abasic site. Remarkable differences in reactivity of this DNA polymer are evident. Note that gel shift assays were carried out for proteins with both **1** and **1a** under conditions used to examine long-range charge transport. From these assays, conditions for specific versus nonspecific binding could be established. Also noteworthy, as described previously (*13*), was a small extent of damage within the protein-binding site that correlated directly with protein affinity measured by gel shift.

First, in the absence of protein, significant damage is apparent at the first 5′-G contained within the 5′-GXGC-3′ run (X = abasic site). In all likelihood, this is the result of the two bases on either side of the abasic site collapsing together so as to optimize π-stacking interactions. Like the Trp−5′-G interaction, this too may be viewed as a structural homologue of a 5′-GG-3′ site. Consistent with this notion, increasing concentrations of wild-type M.*Hha*I effectively turn off the damage at the 5′-G; protein binding and glutamine insertion interfere with guanine−guanine stacking. Moreover, the extent to which damage is turned off is directly related to the amount of M.*Hha*I−**1a** complex generated, established by gel shift. Binding of M.*Hha*I Q237W to **1a**, as one would expect, leads to a different effect. With increasing amounts of M.*Hha*I Q237W−**1a** complex formed, the amount of damage and 5′-G selectivity of damage within the protein−DNA interface is instead enhanced relative to reactions conducted without enzyme; protein binding and Trp insertion make stacking 3′ to the G more facile. Importantly, unlike the experiments with M.*Hha*I Q237W binding to **1**, for **1a**, damage at the distal 5′-GG-3′ is significantly reduced relative to the reaction devoid of enzyme. In addition, the extent of CT-dependent damage seen at the 5′-G of the protein-binding site directly correlates with the extent of specific protein−DNA complex generation. We reconcile

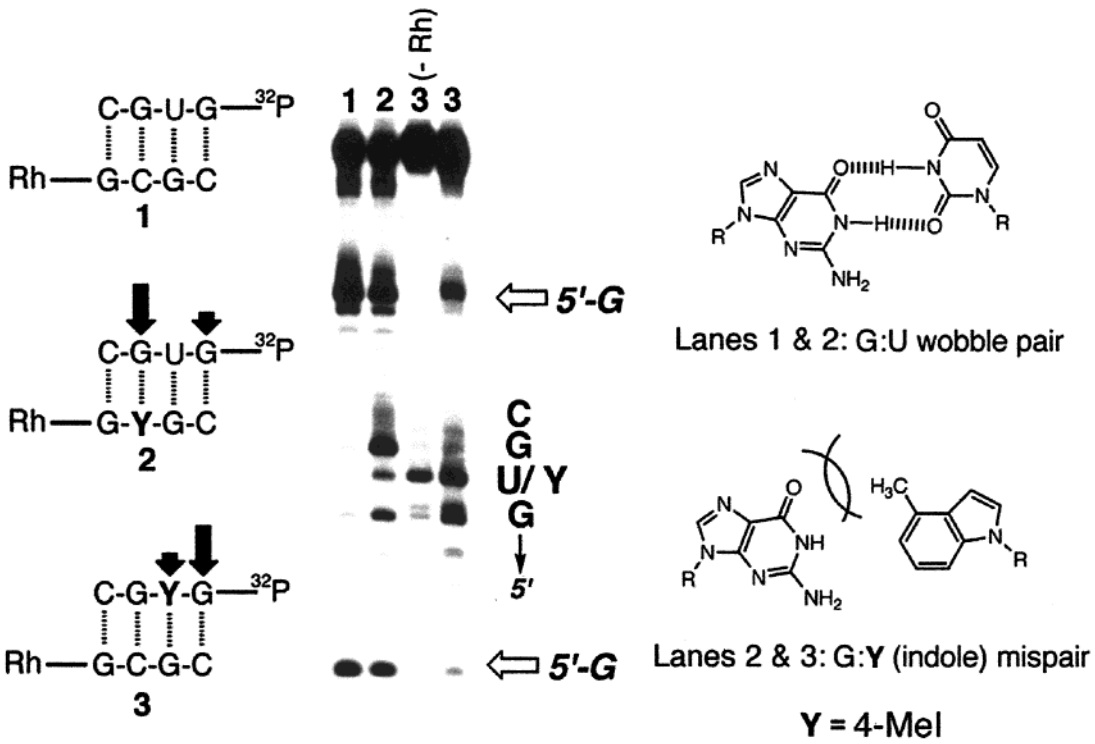

FIGURE 4: Schematics illustrating the M.*Hha*I-binding site of **1** and indole-substituted variants as well as a result of photooxidation of these assemblies. Lane 1 of the phosphorimage shows the charge-transfer damage observed upon 365 nm irradiation of substrate **1** and subsequent piperidine digestion at 90 °C; lane 2, the results for **2**. Both lanes labeled 3 were irradiated and worked up analogously to lanes 1 and 2 except lane 3 marked (−Rh) did not possess a rhodium complex tethered to the duplex. To the right are shown structures of the G:U wobble pair possible with DNA substrates **1** and **2** and the G:indole mispair incorporated within substrates **2** and **3**. The damage encountered at the internal (3′) G of substrate **2** may be the result of either enhanced solvent accessibility of the mismatched G or a lowered ionization potential for this residue resulting from structural disruptions. The 5′-G damage seen with **3** suggests that indole stacking with this G helps to localize the radical to this G and parallels the damage pattern found with M.*Hha*I Q237W.

these data based upon the particularly high yield of radical localized on the 5′-G and Trp residue in this assembly. In fact, spectrosopic results, showing both guanine and Trp radical characterization by transient absorption spectroscopy, confirm this localization. Moreover, with the abasic site substrate, it is also likely that Trp insertion does not lead to a continguous stacking within the DNA duplex.

Also evident only with the TRP237 mutant was charge-dependent damage at the 5′-G contained within the enzyme-binding sequence (Figure 2). We reasoned this damage to be the result of a lowering of the oxidation potential of the G on the 5′-side of the Trp insertion site in a manner similar to that found for the 5′-G of 5′-GG-3′ doublets (*4*, *5*). Indeed molecular modeling of the minimized M.*Hha*I Q237W bound to base-flipped DNA revealed a geometry similar to that for the 5′-GG-3′, placing the indole nitrogen of Trp directly beneath the bicyclic olefin of the 5′-G within the binding site.

We further probed the effects of indole stacking within the duplex by incorporating a nonnatural nucleotide, a 4-methylindole (4-MeI), into either the Rh strand or the ^{32}P-tagged target strand of **1** (Figure 4) (*21*). Although not a rigorous structural analogue of Trp, this served as a means of further exploring whether the 5′-G damage seen with M.*Hha*I Q237W might be accounted for through indole stacking. Figure 4 depicts 4-MeI-substituted variants of **1** (only M.*Hha*I-binding sites shown) and the cleavage pattern for each DNA following irradiation at 365 nm and subsequent treatment with hot piperidine. Irradiation of **1** afforded no damage within the M.*Hha*I-binding site, although significant damage at the 5′-GG-3′ sites was apparent. Placement of the indole moiety opposing the 3′-G in the recognition site on the labeled strand led to extensive damage within the binding site (DNA **2**). Both the first 5′-G and its neighboring uracil were damaged; the guanine displayed a slightly greater piperidine lability. Significant damage was also observed at the central 3′-G of the binding site. This may be the result of this guanosine being paired to the Rh strand indole; guanines involved in G:A mismatches have been shown to be particularly prone to long-range damage, and this may reflect a similar enhancement in the oxidative susceptibility of guanine (*7*). Most important, however, is the result found for 4-MeI-substituted DNA **3**. Although the indole nucleotide itself displays some photoreactivity in the absence of tethered $[Rh(phi)_2(bpy')]^{3+}$, a high degree of selective CT-dependent damage 5′ to the 4-MeI was observed with assembly **3**. This supports the contention that indole−G interactions present with M.*Hha*I Q237W can lead to the 5′-G damage seen within the binding region of **1** and **1a**. Also noteworthy is that we did not observe charge-dependent damage throughout the DNA-binding site in a manner like that seen for **2** with the TRP237 variant of M.*Hha*I; this may indicate that with M.*Hha*I Q237W the uracil or abasic sites of **1** and **1a** serve as preferred sites of base-flipping (*19*, *21*).

Effects on DNA Charge Transport of Binding TATA-Binding Protein (TBP). Inhibition of DNA-mediated CT can also arise upon binding of proteins which disturb DNA stacking through the bending of DNA. TBP plays a pivotal role in transcription initiation; its binding to the sequence

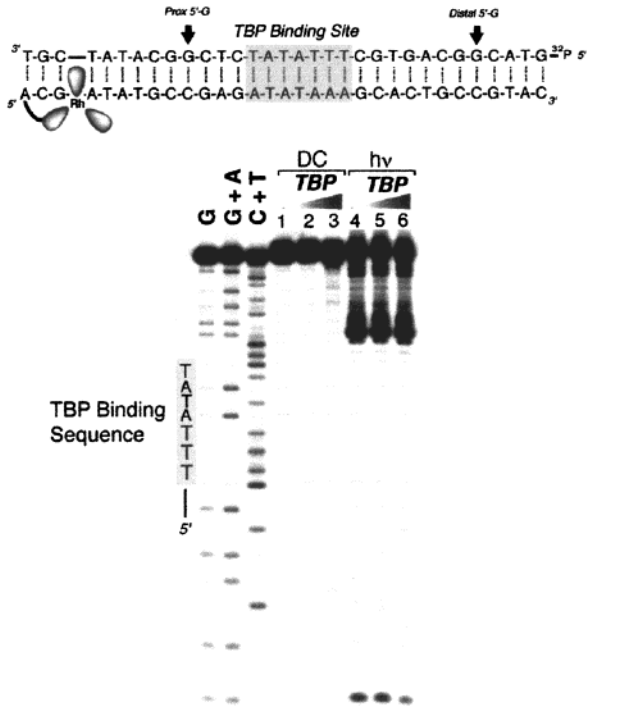

FIGURE 5: Long-range oxidative DNA damage as modulated by binding TBP. Above is schematically illustrated the Rh−DNA assembly with the TATA box recognition site intervening between the proximal and distal 5′-GG-3′ sites. Below the phosphorimagery following photooxidative damage as a function of TBP concentration is shown. Maxam−Gilbert sequencing lanes are as noted. Lanes 1−3 showed dark control samples containing DNA assemblies and 0, 18, and 918 nM TBP, respectively, which were incubated at ambient temperature for a total of 2 h but in the absence of light. Lanes 4−6 showed the results of photooxidation of the DNA assembly in the presence of 0, 18, and 918 nM TBP, respectively, which were irradiated 1 h with 365 nm light after a 1 h preincubation in the absence of light. All samples were treated with piperidine digestion at 90 °C prior to electrophoresis. Analysis of distal/proximal damage ratios reveals that TBP binding induces a roughly 50% inhibition of long-range CT.

5′-TATAAA-3′ helps to nucleate a multisubunit complex vital for the action of RNA polymerase (*22*). Crystallography reveals that, in binding to its consensus sequence, the protein induces two ∼90° kinks at either end of the recognition site (*23*). At each kink, there are extensive phenylalanine−base stacking interactions, but there is no contiguous stacking.

To test the effects of TBP binding upon long-range DNA-mediated CT, we prepared an assembly containing the tethered rhodium photooxidant, proximal and distal 5′-GG-3′ sites, and an intervening TBP-binding site. As illustrated in Figure 5, at the highest TBP concentration there is roughly a 50% decrease in distal guanine damage with binding of TBP to the intervening site; the distal/proximal ratio in guanine oxidation is 0.069 in the absence of protein and 0.036 in the presence of protein. The damage ratio in the presence of 18 nM TBP was essentially that obtained in the absence of TBP, not surprising given the lack of significant DNA−protein binding at low TBP concentration. It should be noted, however, that even in the absence of TBP, the distal/proximal ratio is small compared to that for other random sequences. This low ratio even without protein may reflect the inherent flexibility associated with the 5′-TATA-3′ sequence. Certainly the poor efficiency of charge transport through the 5′-TATA-3′ sequence is well documented (*2*, *3*, *24*). Despite this low ratio, however, binding of the TBP protein further attenuates long-range CT. These results, then, support the conclusion that it is a perturbation in base stacking, as may be caused either by base flipping or through protein-promoted kinking, that leads to the inhibition of DNA-mediated charge transport.

Effects on DNA Charge Transport of Binding the Restriction Endonuclease PvuII. We also were interested in exploring perturbations associated with site-specific binding, but not cleavage, by a restriction endonuclease. An example from this class is the restriction endonuclease R.*Pvu*II; the R.*Pvu*II−DNA complex has been crystallographically characterized (*25*). This restriction enzyme does not significantly distort the π-stack of DNA in any fashion, as a result of either base flipping or kinking.

Figure 6 shows the Rh−DNA assembly constructed to examine how this structurally nondisruptive enzyme modulates CT through DNA as well as the results of photooxidation. As evident by phosphorimagery and in the companion plot of the distal/proximal guanine damage, the ratio of distal/proximal damage increases with increasing enzyme concentration. Parallel native gel shift assays in the presence of 5 mM $CaCl_2$ revealed that nearly quantitative DNA binding was observed at protein concentrations of 2 μM. Notably, R.*Pvu*II under the buffer and concentration conditions described here consistently bound its DNA−Rh assembly without any ensuing endonucleolytic activity. Furthermore, the complexes observed by gel shift were reproducibly consistent with specific binding interactions. Clearly then, specific binding by R.*Pvu*II enhances the ability of the DNA assembly to transport a remotely injected radical cation hole to effect oxidative damage at a distance.

Effects of Antennapedia Homeodomain Protein (ANTP) Binding to DNA-Mediated Charge Transfer. Figure 7 shows the influence upon long-range charge transport of binding a transcription factor to DNA via a helix−turn−helix structural motif. The Antennapedia homeodomain protein plays an important role in cellular differentiation within Drosophila (*26*). This protein, in contrast to those described already, recognizes an extended consensus sequence: 5′-CAAGC-CATTAGAG-3′. Composed of 3 α-helices, with 1 β-turn between helices 2 and 3, the 60 amino acid polypeptide ANTP binds the major groove of DNA through a helix−turn−helix motif. Unlike many other homeodomain proteins, molecular dynamics analysis and NMR studies have shown the ANTP−DNA complex to be very dynamic (*27*). Indeed, it has been proposed that ANTP recognizes its binding site by a fluctuating network of short-lived contacts that avert the entropic cost of having to immobilize side chains on DNA binding.

As shown in Figure 7, binding of ANTP to its Rh−DNA assembly did not promote an inhibition of charge transport. Gel electrophoresis shows strong oxidative damage not only at the proximal 5′-GG-3′ doublet but also at the 5′-GAG-3′ site at the edge of the binding site of the protein. Theoretical calculations predict also a low oxidation potential for such sites (*4*). Importantly, however, there is no systematic change in damage at this site with increasing protein concentration. There was, however, an increase in damage at the distal site at high protein concentration. Effectively, then, increasing concentrations of this protein, with tight binding to the DNA helix, also promote a small increase in long-range charge

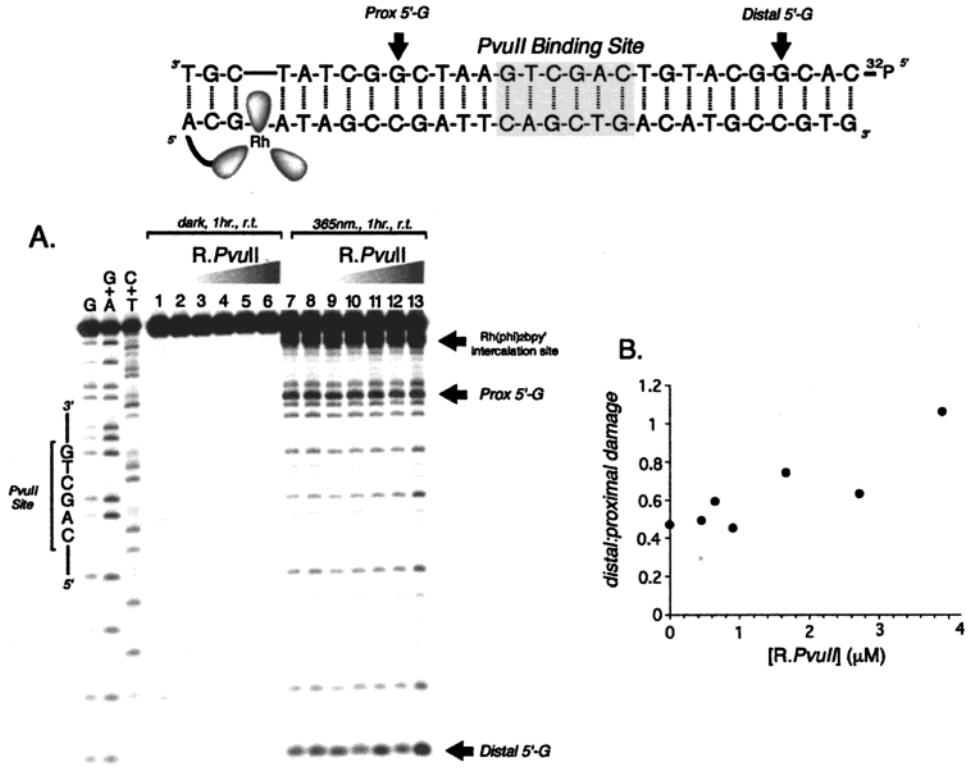

FIGURE 6: Long-range oxidative DNA damage as modulated by binding R.*Pvu*II. Above is schematically illustrated the Rh−DNA assembly with the R.*Pvu*II recognition site intervening between the proximal and distal 5′-GG-3′ sites. Below in (A) the phosphorimagery following photooxidative damage as a function of R.*Pvu*II concentration is shown, and in (B), the distal/proximal guanine damage as a function of bound protein is plotted. In (A), Maxam−Gilbert sequencing lanes are as noted. Lanes 1−6 showed dark control reactions containing 0.45, 0.65, 0.9, 1.7, 2.7, 3.9 μM R.*Pvu*II, respectively, incubated at ambient temperature for 1 h in the absence of light. Lanes 7−13 contained 0, 0.45, 0.65, 0.91, 1.67, 2.72, 3.91 μM R.*Pvu*II, respectively, and were irradiated 1 h with 365 nm light. Samples were treated with piperidine digestion at 90 °C prior to electrophoresis. Parallel native gel electrophoresis was conducted to ensure that under the incubation conditions, the Rh−DNA array was bound with increasing efficiency over the R.*Pvu*II concentration range examined. Graphical analysis of distal/proximal damage ratios (after correction for background damage) shown in panel B reveals that R.*Pvu*II binding actually improves the ability of the *Pvu*II Rh−DNA assembly to support long-range charge transfer.

transport. The results for ANTP, a protein that binds DNA without promoting structural distortion, therefore resemble those obtained with R.*Pvu*II. In binding such proteins, charge transport through the helix is either preserved or, in fact, enhanced. Enhancement correlates particularly well with high (micromolar) concentrations of protein which afford essentially quantitative protein−DNA complexation as assayed by gel shift.

DISCUSSION

These results illustrate routes both to enhance and to inhibit DNA CT through the binding of proteins site-specifically. A strategy to inhibit DNA CT is one involving the utilization of proteins which interrupt base pair stacking within the helix. In contrast, nucleoprotein interactions, which may be considered to enhance or preserve stacking within the double helix, lead to an increase in efficiency of CT.

Reactions with base-flipping enzymes and proteins that kink the DNA, as does TBP, provide clear examples of how proteins may inhibit DNA-mediated CT. Binding of these proteins leads at least to a 50% diminution in long-range oxidative damage. In the case of the base-flipping enzyme M.*Hha*I, for example, we observed that the extent of inhibition depended upon the side chain inserted by the protein within the stack. With the wild-type enzyme, where a glutamine is inserted, the π-stacked array is interrupted, and inhibition of CT results. Alternatively, in the mutant enzyme, where instead a Trp side chain is inserted, more complex effects are evident. In the one substrate, the aromatic heterocyclic indole of the Trp serves to preserve the π-stacked array, and hence long-range oxidative damage is similarly preserved. With the alternate abasic site-containing substrate, maintaining a contiguous π-stack may occur, but the tryptophan interaction with the M.*Hha*I-binding sequence very likely generates a low energy potential well leading to very selective oxidation at the 5′-G within the binding sequence, and hence CT outside of the binding site is not apparent. The capacity of M.*Hha*I Q237W to bind DNA with concomitant CT-dependent oxidative damage has been confirmed also, using transient absorption spectroscopy, where a mixture of Trp and guanine radicals are detected (*16*). Once again, it is important to note that both Trp and guanine radicals generated in such systems originate from a remotely bound metal species, thus highlighting the importance that DNA-mediated CT may play a role in cellular events such as carcinogenesis or redox-based signal transduction (*16*).

Activated damage at the guanine 5′ to Trp insertion is interesting also in another context. This activated chemistry illustrates how the binding of a protein may serve to affect the oxidation potential of specific sites within DNA. We observed a similar activation of guanine by including an unnatural base, the 4-Me indole moiety, at the 3′-site. Hence,

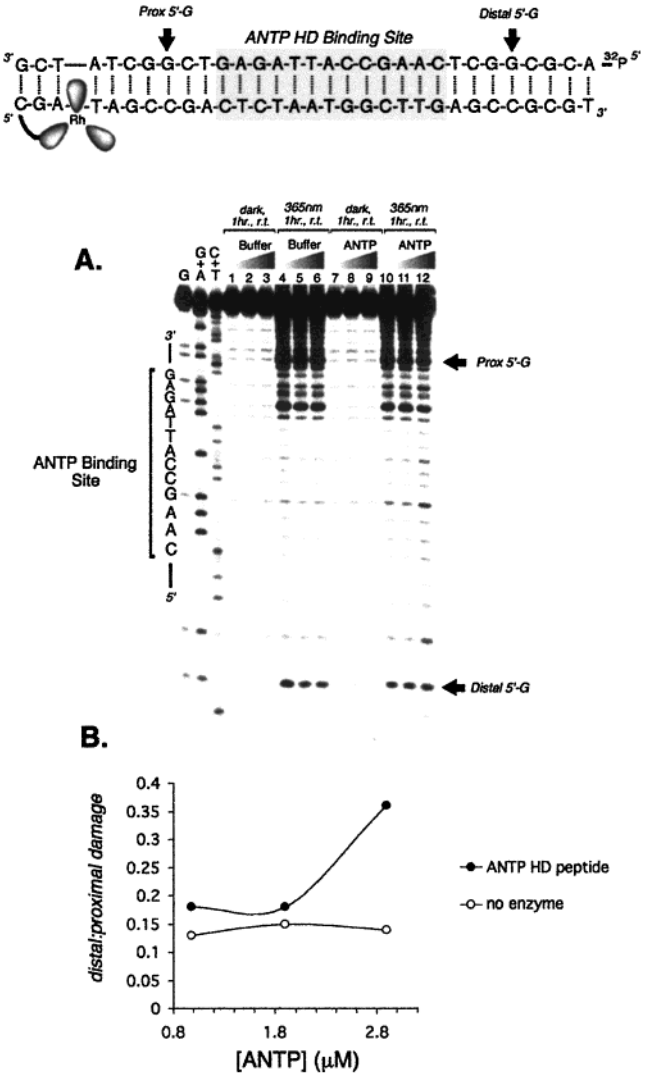

FIGURE 7: Long-range oxidative DNA damage as modulated by binding ANTP. Above is schematically illustrated the Rh−DNA assembly with the ANTP recognition site intervening between the proximal and distal 5′-GG-3′ sites. In (A), the phosphorimagery following photooxidative damage as a function of ANTP concentration is shown, and in (B), the distal/proximal guanine damage with bound protein or in the absence of protein but with increasing protein buffer is plotted. In (A), Maxam−Gilbert sequencing lanes are as noted. Subjection to light or dark conditions is also as noted above each lane. Lanes 1−3 contained amounts of ANTP storage buffer analogous to reactions with 980 nM, 1.9 μM, and 2.9 μM ANTP, respectively. Lanes 4−6 were identical in composition to lanes 1−3 except these reactions were irradiated at 365 nm for 1 h prior to piperidine digestion Lanes 7−9 contained 980 nM, 1.9 μM, and 2.9 μM ANTP, respectively, as did lanes 10−12. Only those ANTP reactions analyzed in lanes 10−12 were irradiated, however. Both CT and gel shift trials (data not shown) were ~170 nM in Rh−DNA and contained 2.1 mM NH_4OAc (pH 8.5), 1.7 mM $KHPO_4$, 8.3 mM NaCl, 80 μM EDTA, 8% glycerol. Following incubation (±light), all samples were brought to 100 μL volume with DDH_2O followed by ethanol precipitation and digestion at 90 °C with 1 M piperidine for 30 min. Graphical analysis of distal/proximal damage ratios (after correction for background damage) shown in panel B reveals that ANTP binding improves the ability of the ANTP Rh−DNA assembly to support long-range charge transfer.

protein binding to specific sites may be used as a strategy not only to perturb π-stacking and CT but also to affect the inherent reactivity of sites in DNA to electron-transfer chemistry.

How DNA-binding proteins enhance DNA CT through their binding in the groove of DNA may be more subtle. Our observations certainly correlate with the exquisite sensitivity in DNA CT to stacking that has been documented (*3*). It is clear that for proteins which bind DNA without perturbing the base stack significantly, no diminution in long-range oxidative damage is found, and this is understandable. However, we find a small but systematic *enhancement* in long-range CT with binding of R.*Pvu*II. This increase is most significant at high protein stoichiometry, as evidenced also by our results with ANTP. Although nonspecific protein interactions are certainly possible under such conditions, it is likely that such interactions would be significantly weaker than those characteristic of specific binding. Indeed, the results of gel shift experiments for each protein system described herein bear this out. These interactions likely restrict the dynamic motions of the DNA bases, thus enhancing the capacity of a nondistorted protein-bound π-stack for CT. In ultrafast measurements, we have found CT through DNA to be gated by dynamic motions within the stack (*28*). Furthermore, we have seen long-range oxidative damage to be stabilized through the tight packing of DNA helices against one another in double-crossover assemblies (*29*).

Measurements of DNA CT as a function of protein binding may therefore be useful as a diagnostic tool to explore how new DNA-binding proteins affect DNA structure (*30*). Currently, making determinations about base flipping, kinking, or even of groove binding is difficult without high-resolution structural information. Clearly, measurements of DNA CT could not be used to distinguish, for example, base flipping from kinking. Conclusions could be drawn, nonetheless, about whether protein binding is associated with the introduction of helical distortions. These data are not likely to be useful in making quantitative assessments of the extent of helical distortion, however. Our results with TBP perhaps best highlight this difficulty. Here, low ratios of distal/proximal damage were evident even without bound protein owing to the inherent flexibility associated with the TATA sequence. Likely, this inherent sequence flexibility also contributes to protein binding (*22*). Nonetheless, the sensitivity of DNA CT to the structural perturbations associated with protein binding may render this chemistry a valuable and unique diagnostic tool.

Given this, it is interesting to note that the decreases or enhancements in CT shown here are quite modest, typically a factor of about 2. Why is there such a relatively small change? We believe this may be telling us something about the importance of DNA base dynamics, structure, and base ionization potentials. First, although protein−DNA interactions affect DNA structure and dynamics, some stacking within the helix remains. These proteins surely do not denature the DNA. Hence, some pathway for charge transport is maintained. Moreover, these data indicate that protein binding does not serve significantly to alter the ionization potential of bases within a given sequence. Indeed, the ionization potential of a given DNA sequence plays just as large a role in a given duplex's capacity for CT as do dynamic motions. Saito and co-workers have rigorously shown that DNA bases within different sequence contexts possess very different ionization potentials and that ionization potentials play a large role in the capacity for a given DNA

duplex to allow CT (*24*). Not only then have these studies highlighted a new methodology for examining protein−DNA-binding interactions, but they also hint at interesting mechanistic caveats pertinent to DNA-mediated CT.

Last, it may be useful to consider the modulation of DNA CT by proteins in the context of reactions within the cell. It is tempting, in light of these findings, to consider that electron-transfer pathways involving nucleic acids and proteins may represent one means of macromolecular communication. Specific protein binding can either activate or inhibit chemical reactions at a distance. These data, then, may lend support to the intriguing possibility that DNA-mediated charge transport may play a physiological role.

ACKNOWLEDGMENT

We thank our close co-workers Sanjay Kumar and Richard J. Roberts of New England Biolabs (Beverly, MA) for samples of wild-type and M.*Hha*I Q237W. We also thank Professor Carl S. Parker (Caltech) for the generous gift of ANTP-binding domain peptide and Professors John Horton and Xiaodong Cheng of Emory University for samples of R.*Pvu*II.

REFERENCES

1. Kelley, S. O., and Barton, J. K. (1999) *Met. Ions Biol. Syst. 36*, 211−249; (b) Rajski, S. R., Jackson, B., and Barton, J. K. (2000) *Mutat. Res. 447*, 49−72; (c) Schuster, G. B. (2000) *Acc. Chem. Res. 33*, 253−260; (d) Geise, B. (2000) *Acc. Chem. Res. 33*, 631−636.
2. (a) Núñez, M. E., Hall, D. B., and Barton, J. K. (1999) *Chem. Biol. 6*, 85−97; (b) Ly, D., Sanii, L., and Schuster, G. B. (1999) *J. Am. Chem. Soc. 121*, 9400−9410.
3. (a) Williams, T. T., Odom, D. T., and Barton, J. K. (2000) *J. Am. Chem. Soc. 122*, 9048−9049; (b) Kelley, S. O., Holmlin, R. E., Stemp, E. D. A., and Barton, J. K. (1997) *J. Am. Chem. Soc. 119*, 9861−9870; (c) Hall, D. B., and Barton, J. K. (1997) *J. Am. Chem. Soc. 119*, 5045−5046.
4. (a) Sugiyama, H., and Saito, I. (1996) *J. Am. Chem. Soc. 118*, 7063−7068; (b) Saito, I., Nakamura, T., Nakatani, K., Yoshioka, Y., Yamaguchi, K., and Sugiyama, H. (1998) *J. Am. Chem. Soc. 120*, 12686−12687; (c) Sugiyama, H., and Saito, I. (1996) *J. Am. Chem. Soc.118*, 7063−7068.
5. Prat, F., Houk, K. N., and Foote, C. S. (1998) *J. Am. Chem. Soc. 120*, 845.
6. Hall, D. B., Holmlin, R. E., and Barton, J. K. (1996) *Nature 382*, 731−735.
7. Arkin, M. R., Stemp, E. D. A., Pulver, S. C., and Barton, J. K. (1997) *Chem. Biol. 4*, 389−400.
8. (a) Gasper, S. M., and Schuster, G. B. (1997) *J. Am. Chem. Soc. 119*, 12762−12771; (b) Henderson, P. T., Jones, D., Hampikian, G., Kan, Y., and Schuster, G. B. (1999) *Proc. Natl. Acad. Sci. U.S.A. 96*, 8353−8358; (c) Ly, D., Sanii, L., and Schuster, G. B. (1999) *J. Am. Chem. Soc. 121*, 9400−9410; (d) Kan, Y., and Schuster, G. B. (1999) *J. Am. Chem. Soc. 121*, 10857−10864; (e) Sartor, V., Henderson, P. T., and Schuster, G. B. (1999) *J. Am. Chem. Soc. 121*, 11027−11032.
9. (a) Meggers, E., Michel-Beyerle, M. E., and Giese, B. (1998) *J. Am. Chem. Soc. 120*, 12950−12955; (b) Giese, B., Wessely, M., Spormann, M., Lindermann, U., Meggers, E., and Michel-Beyerle, M. E. (1999) *Angew. Chem., Int. Ed. Engl. 38*, 996−998; (c) Meggers, E., Kusch, D., Spichty, M., Wille, U., and Giese, B. (1998) *Angew. Chem., Int. Ed. Engl. 37*, 460−462.
10. (a) Nakatani, K., Dohno, C., and Saito, I. (1999) *J. Am. Chem. Soc. 121*, 10854−10855; (b) Nakatani, K., Dohno, C., and Saito, I. (1999) *J. Org. Chem. 64*, 6901−6904.
11. Hall, D. B., Kelley, S. O., and Barton, J. K. (1998) *Biochemistry 37*, 15933−15940.
12. Núñez, M. E., Noyes, K. T., Gianolio, D. A., McLaughlin, L. W., and Barton, J. K. (2000) *Biochemistry 39*, 6190−6199.
13. Rajski, S. R., Kumar, S., Roberts, R. J., and Barton, J. K. (1999) *J. Am. Chem. Soc. 121*, 5615−5616.
14. (a) Cheng, X., Kumar, S., Posfai, J., Pflugrath, J. W., and Roberts, R. J. (1993) *Cell 74*, 299−307; (b) O'Gara, M., Klimasauskas, S., Roberts, R. J., and Cheng, X. (1996) *J. Mol. Biol. 261*, 634−645.
15. (a) Mi, S., Alonso, D., and Roberts, R. J. (1995) *Nucleic Acids Res. 23*, 620−627; (b) Garcia, R. A., Bustamante, C. J., and Reich, N. O. (1996) *Proc. Natl. Acad. Sci. U.S.A. 93*, 7618−7622.
16. Wagenknecht, H. A., Rajski, S. R., Pascaly, M., Stemp, E. D. A., and Barton, J. K. (2001) *J. Am. Chem. Soc.*, in press.
17. (a) Beaucage, S. L., and Caruthers, M. H. (1981) *Tetrahedron Lett. 22*, 1859−1802; (b) Caruthers, M., Beaton, G., Wu, J. V., and Wiesler, W. (1992) *Methods Enzymol. 211*, 3−20; (c) Goodchild, J. (1990) *Bioconjugate Chem. 1*, 165−187.
18. Holmlin, R. E., Dandliker, P. J., and Barton, J. K. (1999) *Bioconjugate Chem. 10*, 1122−1130.
19. Klimasauskas, S., and Roberts, R. J. (1995) *Nucleic Acids Res. 23*, 1388−1395.
20. O'Gara, M., Horton, J. R., Roberts, R. J., and Cheng, X. (1998) *Nat. Struct. Biol. 5*, 872−877.
21. A closely related analogue of 4-MeI has recently been shown to be well stacked within duplex DNA when paired with a complementary non-hydrogen bonding base. See: Guckian, K. M., Krugh, T. R., and Kool, E. T. (2000) *J. Am. Chem. Soc. 122*, 6841−6847.
22. (a) De Souza, O. N., and Ornstein, R. L. (1998) *Biopolymers 46*, 403−415; (b) Coleman, R. A., Taggart, A. K. P., Benjamin, L. R., and Pugh, B. F. (1995) *J. Biol. Chem. 270*, 13842−13849; (c) Lee, D. K., Horikoshi, M., and Roeder, R. G. (1991) *Cell 67*, 1241−1250.
23. (a) Kim, J. L., Nikolov, D. B., and Burley, S. K. (1993) *Nature 365*, 520−527; (b) Kim, Y., Geiger, J. H., Hahn, S., and Sigler, P. B. (1993) *Nature 365*, 512−520.
24. (a) Meggers, E., Michel-Beyerle, M. E., and Giese, B. (1998) *J. Am. Chem. Soc. 120*, 12950−12955; (b) Nakatani, K., Dohno, C., and Saito, I. (2000) *J. Am. Chem. Soc. 122*, 5893−5894.
25. Cheng, X., Balendiran, K., Schildkraut, I., and Anderson, J. E. (1994) *EMBO J. 13*, 3927−3935.
26. (a) LeRoux, I., Joliot, A. H., Bloch-Gallego, E., and Prochiantz, A. (1993) *Proc. Natl. Acad. Sci. U.S.A. 90*, 9120−9124; (b) Derossi, D., Calvet, S., Trembleau, A., Brunissen, A., Chassaing, G., and Prochiantz, A. (1996) *J. Biol. Chem. 271*, 18188−18193; (c) Affolter, M., Percival-Smith, A., Martin, Muller, M., Leupin, W., and Gehring, W. J. (1990) *Proc. Natl. Acad. Sci. U.S.A. 87*, 4093−4097; (d) Derossi, D., Joliot, A. H., Chassaing, G., and Prochiantz, A. (1994) *J. Biol. Chem. 269*, 10444−10450.
27. (a) Fraenkel, E., and Pabo, C. O. (1998) *Nat. Struct. Biol. 5*, 692−697; (b) Billeter, M., et al. (1993) *J. Mol. Biol. 234*, 1084−1093; (c) Billeter, M., Guntert, P., Luginbuhl, P., and Wuthrich, K. (1996) *Cell 85*, 1057−1065.
28. (a) Fiebig, T., Wan, C. Z., Kelley, S. O., Barton, J. K., and Zewail, A. H. (1999) *Proc. Natl. Acad. Sci. U.S.A. 96*, 1187−1192; (b)Wan, C. Z., Fiebig, T., Kelley, S. O., Treadway, C. R., Barton, J. K., and Zewail, A. H. (1999) *Proc. Natl. Acad. Sci. U.S.A. 96*, 6014−6019.
29. Odom, D. T., Dill, E. A., and Barton, J. K. (2000) *Chem. Biol. 7*, 475−481.
30. Núñez, M. E., Rajski, S. R., and Barton, J. K. (2000) *Methods Enzymol. 319*, 165−188.

BI002684T